

Oxygen and nitrogen abundances of H II regions in six spiral galaxies

A.S. Gusev,¹ L.S. Pilyugin,² F. Sakhibov,³ S.N. Dodonov,⁴ O.V. Ezhkova,¹
M.S. Khramtsova⁵

¹ Sternberg Astronomical Institute, Lomonosov Moscow State University, Universitetsky pr. 13, 119992 Moscow, Russia

² Main Astronomical Observatory of National Academy of Sciences of Ukraine, Zabolotnogo str. 27, 03680 Kiev, Ukraine, pilyugin@mao.kiev.ua

³ University of Applied Sciences of Mittelhessen, Campus Friedberg, Department of Mathematics, Natural Sciences and Data Processing, Wilhelm-Leuschner-Strasse 13, 61169 Friedberg, Germany

⁴ Special Astrophysical Observatory, Russian Academy of Sciences, 369169 Nizhnij Arkhyz, Russia

⁵ Institute of Astronomy, Russian Academy of Sciences, ul. Pyatnitskaya 48, 119017 Moscow, Russia

Accepted 2012 May 15. Received 2012 May 14; in original form 2012 February 29

ABSTRACT

Spectroscopic observations of 63 H II regions in six spiral galaxies (NGC 628, NGC 783, NGC 2336, NGC 6217, NGC 7331, and NGC 7678) were carried out with the 6-meter telescope (BTA) of Russian Special Astrophysical Observatory with the Spectral Camera attached to the focal reducer SCORPIO in the multislit mode with a dispersion of 2.1 Å/pixel and a spectral resolution of 10 Å. These observations were used to estimate the oxygen and nitrogen abundances and the electron temperatures in H II regions through the recent variant of the strong line method (NS calibration). The parameters of the radial distribution (the extrapolated central intercept value and the gradient) of the oxygen and nitrogen abundances in the disks of spiral galaxies NGC 628, NGC 783, NGC 2336, NGC 7331, and NGC 7678 have been determined. The abundances in the NGC 783, NGC 2336, NGC 6217, and NGC 7678 are measured for the first time. Galaxies from our sample follow well the general trend in the luminosity – central metallicity diagram for spiral and irregular galaxies.

Key words: spectroscopy – galaxies: abundances – ISM: abundances – H II regions

1 INTRODUCTION

We have observed emission line spectra of 63 giant H II regions in six spiral galaxies as a part of our study of star formation regions in spiral and irregular galaxies. Giant extragalactic H II regions are the birth places of star clusters and can be used to study the current star formation and chemical abundances in galaxies. Giant H II regions are ionised by clusters of young massive stars. Their sizes range from several tens to ≈ 500 pc, so they are larger and brighter in comparison to Galactic H II regions. Certain selection effects must be noted. Necessarily poorer spatial resolution contributes to a tendency to identify larger regions in more distant galaxies; at better resolution these regions break up into groups or chains of smaller clumps (Dinerstein 1990).

One of the main interests in H II regions is in the study of elemental abundances and their gradients in galaxies. A large number of regions have been observed for this purpose (Zaritsky et al. 1994; Roy et al. 1996; van Zee et al. 1998; Dutil & Roy 1999; Kennicutt et al. 2003; Bresolin et al. 2005, 2009, among others). Radial distributions of oxygen and nitrogen abundances across the disks are mandatory in investigations of different aspects of formation and evolution of spiral galaxies. The measurement of the distribution of elemental abundances within galaxies is a tool for studying galaxy formation and evolution. There are several investi-

gations of possible relationship between the abundances properties and global characteristics of galaxies such a Hubble type and luminosity (Pagel 1991; Vila-Costas & Edmunds 1992; Dutil & Roy 1999; Garnett & Shields 1987). The oxygen abundance in the interstellar gas is usually used as a tracer of metallicity in late type (spiral and irregular) galaxies at the current epoch. The study of abundance gradients in the disk of spiral galaxies has been started by Searle (1971), with the recognition of a radial abundance gradient in M33. Results of investigations of variations in the gas composition within galaxies combined with results on the evolution of stellar populations provide the development of chemical evolution models (Chiappini et al. 2003; Marcon-Uchida et al. 2010).

A study of abundances and their gradients is based on measurements of emission line spectra of individual H II regions in nearby galaxies. To define the parameters of radial distribution of oxygen and nitrogen abundances (the extrapolated central intercept value and the gradient), the abundance measurements for a sufficiently large number of H II regions evenly distributed across the galaxy disk are necessary. Measurements of this kind are available for the limited number (~ 50) of nearby galaxies (see compilations in Garnett 2002; Pilyugin et al. 2004; Moustakas et al. 2010).

Here we report spectra of 63 H II regions in a sample of six spiral galaxies: NGC 628, NGC 783, NGC 2336, NGC 6217,

Table 1. The galaxy sample.

Galaxy	Type	B_t (mag)	RA ^a (J2000.0)	DEC ^a (J2000.0)	Inclination (degree)	P.A. (degree)	v^b (km/s)	R_{25}^c (arcmin)	R_{25}^c (kpc)	d (Mpc)	M_B (mag)
1	2	3	4	5	6	7	8	9	10	11	12
NGC 628	Sc	9.70	01 36 41.81	+15 47 00.3	7	25	659	5.23	10.96	7.2	-20.72
NGC 783	Sc	13.18	02 01 06.59	+31 52 56.2	43	57	5192	0.71	14.56	70.5	-22.01
NGC 2336	SB(R)bc	11.19	07 27 03.98	+80 10 41.1	55	175	2202	2.51	23.51	32.2	-22.14
NGC 6217	SB(R)bc	11.89	16 32 39.28	+78 11 53.6	33	162	1368	1.15	6.89	20.6	-20.45
NGC 7331	Sbc	10.20	22 37 04.16	+34 24 56.0	75	169	818	4.89	20.06	14.1	-21.68
NGC 7678	SBC	12.50	23 28 27.87	+22 25 14.0	44	21	3488	1.04	14.46	47.8	-21.55

^a Coordinates of the galaxy center. Units of right ascension are hours, minutes, and seconds, and units of declination are degrees, arcminutes, and arcseconds.

^b Heliocentric radial velocity. ^c Isophotal radius (25 mag/arcsec² in the B -band) corrected for Galactic extinction and absorption due to the inclination of a galaxy.

Table 2. Journal of observations.

Object (Pos. ^a)	Date	Exposures (s)	Seeing (arcsec)	Airmass
NGC 628 (1)	2008.02.07	900 × 2	1.9	2.03
NGC 783 (1)	2006.10.19	900 × 3	3.0	1.28
NGC 783 (2)	2007.09.07	900 × 4	1.6	1.02
NGC 783 (3)	2008.02.09	900 × 6	1.9	1.29
NGC 2336 (1)	2006.10.19	900 × 4	2.0	1.39
NGC 2336 (2)	2008.02.08	900 × 8	1.4	1.31
NGC 2336 (3)	2006.10.19	300 + 900	2.0	1.32
NGC 2336 (4)	2008.02.09	900 × 6	1.2	1.33
NGC 6217 (1)	2006.08.23	900 × 4	1.8	1.47
NGC 7331 (1)	2006.08.23	900 × 4	2.1	1.17
NGC 7678 (1)	2006.08.22	900 × 3	1.4	1.15
NGC 7678 (2)	2006.10.19	900 × 2	1.6	1.08
NGC 7678 (3)	2006.10.19	900 × 3	1.6	1.08

^a Slit position

NGC 7331, and NGC 7678. A first motivation of the spectral observations is the determination of the oxygen and nitrogen abundances and electron temperatures in individual H II regions using the recent NS- and ON calibration (Pilyugin et al. 2010; Pilyugin & Mattsson 2011). The abundances will be used in the computation of the grid of evolutionary models of star clusters embedded in studied H II regions. The second motivation is the determination of the optical extinction by dust to the gas, from the measured Balmer decrement in the studied H II regions.

In this paper we describe observations and data reduction, the derivation of elemental abundances, electron temperatures and optical extinction for individual H II regions and the examination their radial gradients across the disks. Results of these examinations provide information about the chemical abundance of interstellar medium from which embedded stars formed, as well as the dust extinction estimations in the surrounding gas.

The paper is organized as follows. The observations and data reduction are described in Section 2. The oxygen and nitrogen abundances and the electron temperatures for individual H II regions as well the parameters of the radial distributions (the extrapolated central intercept value and the gradient) of the oxygen and nitrogen abundances and electron temperature in galaxies are discussed in Section 3. Section 4 gives a brief summary.

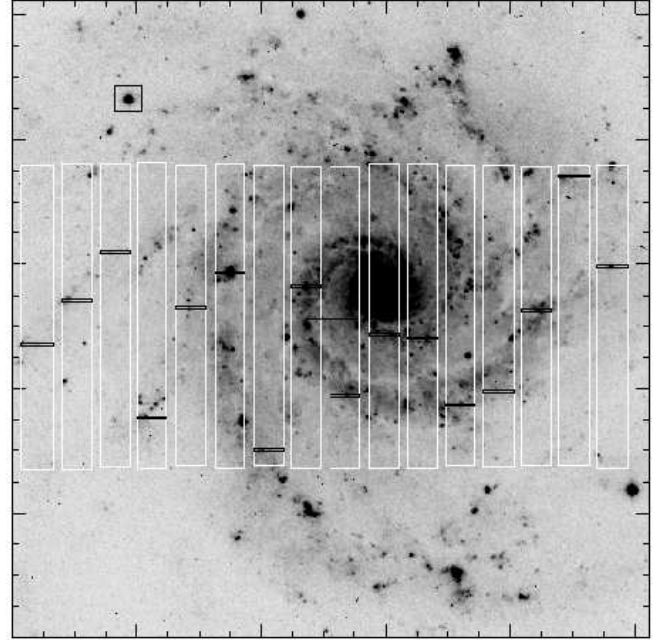


Figure 1. Disposition of 16 slits (black small horizontal rectangles) for NGC 628. North is upward and east is to the left ($P.A._{slits} = 90^\circ$). The size of the image is 6.1×6.1 arcmin². The black square shows a guide star for the exposures.

Throughout the paper, we will be using the following notations for the line fluxes,

$$R_2 = [\text{O II}]\lambda 3727 + \lambda 3729 = I_{[\text{OII}]\lambda 3727 + \lambda 3729} / I_{\text{H}\beta}, \quad (1)$$

$$N_2 = [\text{N II}]\lambda 6548 + \lambda 6584 = I_{[\text{NII}]\lambda 6548 + \lambda 6584} / I_{\text{H}\beta}, \quad (2)$$

$$S_2 = [\text{S II}]\lambda 6717 + \lambda 6731 = I_{[\text{SII}]\lambda 6717 + \lambda 6731} / I_{\text{H}\beta}, \quad (3)$$

$$R_3 = [\text{O III}]\lambda 4959 + \lambda 5007 = I_{[\text{OIII}]\lambda 4959 + \lambda 5007} / I_{\text{H}\beta}. \quad (4)$$

The electron temperatures t are given in units of 10^4K .

2 OBSERVATIONS AND REDUCTION

We selected galaxies with known $UBVRI$ photometry of H II regions, obtained by our team in the previous works: NGC 628 (Bruevich et al. 2007), NGC 783 (Gusev 2006a,b), NGC 2336 (Gusev & Park 2003), NGC 6217 (Artamonov et al. 1999),

Table 3. Offsets, galactocentric distances, radial velocities of H II regions.

H II region	Pos. ^a	Ref. ^b	N-S ^c (arcsec)	E-W ^c (arcsec)	r^d (kpc)	v^e (km/s)
NGC 628						
1	1	94, 54	+12.5	+129.0	4.55	620
2	1	92	-12.0	+87.7	3.11	665
3	1	77, 58	-64.3	+36.5	2.58	611
4	1	75	-65.4	+45.0	2.77	638
5	1	73, 11	-28.8	+25.3	1.34	654
6	1	25, 6	+0.2	-43.0	1.51	655
7	1	62, 81	-91.8	-68.1	4.01	628
8	1	58	-72.0	-132.6	5.31	614
9	1	35	+19.7	-153.1	5.42	716
10	1	38, (5)	-6.4	-177.9	6.25	711
NGC 783						
1	1	—	-24.3	+16.0	10.60	5181
2	1	—	-27.5	+23.7	12.83	5202
3	1	—	-4.8	-19.7	8.33	5192
4	1	—	+19.5	-29.1	11.96	5235
5	2	—	-19.5	+22.1	10.17	5270
6	2	—	-20.0	+25.6	11.15	5103
7	2	—	+21.6	-28.3	12.20	5153
8	3	—	+5.1	-22.9	8.42	5233
NGC 2336						
1a	1	—	-113.8	+33.5	20.79	2011
1b	2	—	-113.8	+33.5	20.79	2048
2	1	28	-89.0	-40.0	16.89	2006
3	1	27a	-71.8	+0.2	11.30	2040
4a	1	26	-47.8	-10.5	7.79	2009
4b	4	26	-47.8	-10.5	7.79	2052
5	1	22	-27.5	-9.8	4.86	2028
6	1	17	+17.5	+85.4	23.02	2264
7a	1	5	+95.9	+13.6	15.19	2432
7b	2	5	+95.9	+13.6	15.19	2410
8	2	27d	-82.5	-9.5	12.99	2013
9	2	—	-62.6	+8.1	10.27	1917
10a	2	19	+3.4	+43.8	11.82	2141
10b	4	19	+3.4	+43.8	11.82	2198
11	2	16	+18.2	+38.7	10.59	2349
12	2	10	+52.3	+0.2	8.22	2512
13	2	8	+68.1	-34.5	14.84	2485
14a	2	2	+142.0	-11.5	22.83	2573
14b	4	2	+142.0	-11.5	22.83	2545
15a	3	30	-109.0	-32.1	18.49	1940
15b	4	30	-109.0	-32.1	18.49	1935
16a	3	27b	-77.3	-3.6	12.11	2014
16b	4	27b	-77.3	-3.6	12.11	2018
17a	3	21	-26.1	+48.3	14.05	2167
17b	4	21	-26.1	+48.3	14.05	2061
18	4	29	-94.5	-37.3	17.18	2233
19	4	27e	-83.9	-4.3	13.13	2064
20	4	—	-31.6	+48.6	14.49	2160
21	4	—	-19.3	+47.6	13.50	1982
22	4	—	+27.2	-62.7	17.88	2364
23	4	15	+24.4	-61.7	17.47	2263
24	4	9	+62.6	+48.3	15.61	2375
25	4	—	+67.7	+44.5	15.32	2443
26	4	—	+77.7	-5.3	12.43	2575
27	4	7	+80.8	-4.6	12.88	2422
28	4	4	+111.7	-31.1	20.17	2335
NGC 6217						
1	1	—	+29.8	+13.9	3.30	1443
2	1	—	+42.2	+13.0	4.41	1485
3	1	—	-14.6	+23.2	3.24	1348

Table 3. Continued

H II region	Pos. ^a	Ref. ^b	N-S ^c (arcsec)	E-W ^c (arcsec)	r^d (kpc)	v^e (km/s)
NGC 7331						
1	1	—	+123.2	+40.4	9.78	537
2	1	—	+76.8	+18.0	5.45	512
3	1	—	+27.4	+16.2	3.48	667
4	1	1	-50.2	+23.1	9.06	865
NGC 7678						
1	1	—	-54.2	+12.6	13.02	3422
2	1	—	-31.8	-7.1	8.57	3431
3	1	—	-23.3	-14.8	8.10	3525
4	1	—	-14.5	-21.0	8.11	3553
5	1	—	+3.7	-26.6	8.15	3455
6	2	—	-26.5	+14.2	7.02	3412
7	2	—	-10.5	+31.6	9.63	3415
8a	2	—	-15.8	+27.3	8.56	3426
8b	3	—	-15.8	+27.3	8.56	3432
9	3	—	-46.5	-5.2	11.87	3384
10	3	—	-23.0	+6.2	5.56	3398

^a Slit position. ^b H II region number from Belley & Roy (1992) (first number), from Rosales-Ortega et al. (2011) (second number), and from van Zee et al. (1998) (second number in brackets) for NGC 628, from Gusev & Park (2003) for NGC 2336, and from Bresolin et al. (1999) for NGC 7331. ^c Offsets from the galactic centre (see Table 1), positive to the north and west. ^d Deprojected galactocentric distance.

^e Radial velocity of H II region (km s⁻¹).

NGC 7331 (unpublished), NGC 7678 (Artamonov et al. 1997). The galaxy sample is presented in Table 1. The columns show parameters from the LEDA data base (Paturel et al. 2003): morphological type and apparent magnitude of the galaxy in columns (2) and (3), coordinates (epoch 2000) in columns (4) and (5), the inclination and position angles in columns (6) and (7), radial velocity in column (8), the isophotal radius in arcmin and kpc in columns (9) and (10), distance in the column (11), the absolute blue magnitude M_B in column (12).

2.1 Observations

The observations were carried out at the 6 m telescope of Special Astrophysical Observatory (SAO) of the Russian Academy of Sciences with Spectral Camera attached at the focal reducer SCORPIO (Afanasiev & Moiseev 2005) ($f/4 \rightarrow f/2.6$) in the multislit mode; the field was about 6 arcmin and the pixel size was 0.178 arcsec on a EEV 42-40 (2048 × 2048 pixels) CCD detector. The data for six galaxies were acquired during observing runs in 2006–2008 (see the journal of observations in Table 2).

The SCORPIO multislit unit is an arrangement that consists of 16 metal strips with slits located in the focal plane and moved in a 2.9×5.9 arcmin² field (Fig. 1). The size of slits is 1.5×18 arcsec², the distance between centres of neighbouring slits is 22 arcsec.

We used the grism VPHG550G with a dispersion of 2.1 Å/pixel and a spectral resolution of 10 Å, which provided spectral coverage from [O II]λ3727+λ3729 oxygen emission lines to [S II]λ6717+λ6731 sulphur emission lines. The example of spectrum is presented in Fig. 2.

We selected target H II regions using B band and $H\alpha$ CCD images of galaxies, which were obtained with the 1 m and 1.5 m telescopes of the Mt. Maidanak Observatory (Institute of Astronomy,

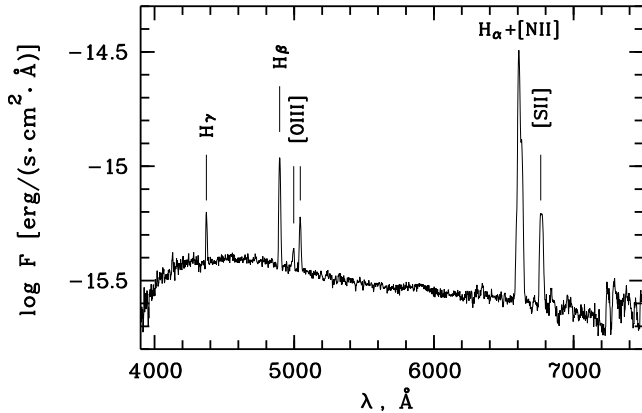


Figure 2. The observed spectrum “b” of the H II region 17 in NGC 2336.

Uzbek Academy of Sciences) in Uzbekistan and with the 1.8 m telescope of the Bohyunsan Optical Astronomy Observatory (Korea Astronomy and Space Science Institute) in Korea.

As mentioned above, the broadband *UBVRI* photometry of selected H II regions, derived previously by us and our colleagues as a part of our study of star formation processes in spiral and irregular galaxies, provided the source of targets for the multi-slit observations. We selected objects widely distributed across the face of the galaxies, enabling the study of the chemical abundance gradients. The H II regions were selected for spectroscopy based on their brightness and size, with typical angular diameters from 2 up to 5 arcsec.

The total exposure time of the set consists of several time intervals. After the every time interval, positions of slits were displaced along the X axes with a step of 20 pixels. X axes runs along the slit and Y axes runs perpendicularly to the slit (see Fig. 1). This technique allows us to obtain spectra of several neighbouring H II regions using the same slit. Therefore, the exposure time for individual H II regions was smaller than the total exposure time of the set indicated in the Table 2.

The observing procedure consisted of obtaining bias, flat and wavelength calibration images at the beginning and the end of the each set. Several spectrophotometric standards were observed during the each night at different air mass.

2.2 Data reduction

Initial data reduction followed routine procedures, including bias, cosmic-ray, flat-field and atmospheric extinction corrections and photometric calibration, intensity normalisation to the intensity of the central (8th) slit, wavelength calibration with a standard He-Ne-Ar lamp, subtracting the background, transformation to one-dimensional spectrum and summing of spectra, using the European Southern Observatory Munich Image Data Analysis System (MIDAS).

The emission line fluxes were measured using the continuum-subtracted spectrum. Flux calibration was performed, using standard stars BD+25°4655, HZ2, HZ4, Feige 34, and G193–74 (Oke 1990). Both, the spectra of standard stars and the SAO astroclimate data of Kartasheva & Chunakova (1978) were used for a calculation of the extinction coefficient and a correction for the atmospheric extinction. The blended lines Hα+[NII]λ6548+λ6584 and

[SII]λ6717+λ6731 were measured by the three or two-Gaussian fitting, respectively.

The extraction aperture corresponded to the area, where brightest emission lines from H II regions were “visible” above the noise. This size is close to the angular diameter of individual H II regions from the imaging surveys as projected along the P.A. of the slit.

Coordinates, deprojected galactocentric distances, and radial velocities are listed in Table 3. Reddening-corrected line intensities $I(\lambda)/I(H\beta)$, underreddened fluxes $F(H\beta)$, and the logarithmic extinction coefficients $c(H\beta)$ are given in Table 4. Though the sulphur lines [SII]λ6717 and [SII]λ6731 were debled in several cases, the accuracy was very low. Therefore the Table 4 presents the sum of the [SII](λ6717+λ6731) of sulphur lines. Some H II regions were observed twice, they are marked with letters “a” and “b” in Tables 3, 4.

Absolute emission-line fluxes derived for the same object in different nights can be differ because of following reasons: a) different seeings in different nights and b) a slight deviation of the slit from the previous position. Note that the apparent sizes of the studied H II regions are generally larger than the width of the slit. It should be noted that, although the absolute emission-line fluxes can differ by a large amount between different observations depending of the exact slit placement, flux ratios derived for the same object on different nights coincide within the errors (see Table 4).

At calculation of the error of the line intensity measurement the following factors have been taken into consideration. The first factor is related to the Poisson statistics of the line photon flux. The second factor of the error appears by the computation of the underlying continuum, and makes the main contribution to the unaccuracy of faint lines. The third factor concerns with the uncertainty of the spectral sensitivity curve. It gives an additional error to the relative line intensities. The last factor is related to the goodness of fit of the line profile and is crucial for blended lines. All these components are summed in quadrature. The total errors have been propagated to calculate the errors of all derived parameters.

Estimations of radial velocities of studied H II regions (last column in Table 3) were derived as a by-product through the measurements of Doppler shifts of Hα line in spectra. The accuracy of radial velocity measurements is about 30 km/s. Analysis of the observed radial velocities is beyond of the scope of this paper.

The measured emission fluxes F were corrected for the interstellar reddening and Balmer absorption in the underlying stellar continuum. We used the theoretical Hα to Hβ ratio from Osterbrock (1989) assuming case B recombination and an electron temperature of 10,000 K and the analytical approximation to the Whitford interstellar reddening law by Izotov et al. (1994). We adopted the absorption equivalent width $EW_a(\lambda) = 2\text{Å}$ for hydrogen lines for all objects, which is the mean value for H II regions derived by McCall et al. (1985). For lines other than hydrogen $EW_a(\lambda) = 0$. The uncertainty of the logarithmic extinction coefficient $c(H\beta)$ is calculated from the measurements errors of Hα and Hβ lines and propagated to the dereddened line ratios.

2.3 Comparison with previous observations

H II regions in the galaxies NGC 628 and NGC 7331 have previously been observed via spectroscopy (McCall et al. 1985; Ferguson et al. 1998; van Zee et al. 1998; Bresolin et al. 1999) or the spectrophotometric imaging (Belley & Roy 1992) or the Integral Field Spectroscopy method (Rosales-Ortega et al. 2011). There is only one overlapping with the previous spectroscopic ob-

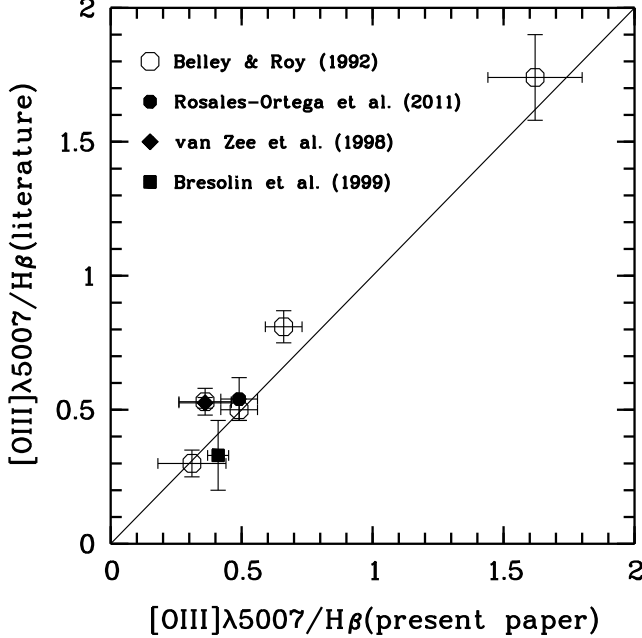
Table 4. The reddening-corrected fluxes of main emission lines of H II regions.

H II region	[O II] ^a 3727+3729	[O III] ^a 5007	[N II] ^a 6584	[S II] ^a 6717+6731	<i>F</i> (H β) ^b 4861	<i>c</i> (H β)
NGC 628						
1	—	—	0.73±0.41	0.42±0.24	7.48±1.17	0.74±0.31
2	—	—	1.06±0.42	1.16±0.45	8.04±0.85	0.58±0.24
3	—	—	0.61±0.26	0.35±0.14	27.40±3.07	0.33±0.21
4	—	0.31±0.13	0.46±0.35	0.54±0.30	5.21±0.79	0.37±0.31
5	—	—	0.70±0.35	0.78±0.35	9.61±1.08	0.30±0.25
6	—	—	—	—	2.12±0.80	0.85±0.96
7	5.64±2.01	0.49±0.07	0.79±0.22	0.47±0.12	33.32±1.82	0.00±0.13
8	4.06±1.74	0.66±0.07	0.77±0.18	0.51±0.10	38.15±2.05	0.12±0.12
9	—	1.62±0.18	0.59±0.16	0.32±0.08	22.62±1.41	0.87±0.13
10	—	0.36±0.10	0.74±0.29	0.77±0.30	30.51±3.80	0.03±0.22
NGC 783						
1	—	1.47±0.20	1.06±0.27	0.72±0.20	5.81±0.38	0.28±0.15
2	—	0.73±0.30	—	—	1.38±0.36	0.08±0.55
3	1.80±0.60	0.23±0.04	1.33±0.20	0.89±0.13	22.15±6.51	0.51±0.09
4	—	0.68±0.13	1.46±0.46	1.19±0.39	3.34±0.29	0.90±0.20
5	2.34±0.68	0.23±0.04	0.54±0.14	0.86±0.15	7.78±0.31	0.61±0.10
6	2.45±0.53	0.44±0.05	1.50±0.21	1.16±0.17	11.69±0.42	0.44±0.09
7	—	1.25±0.46	3.11±1.87	2.30±1.46	2.55±0.46	0.76±0.45
8	2.35±0.54	0.32±0.06	1.16±0.19	0.64±0.12	25.97±1.00	0.73±0.09
NGC 2336						
1a	—	0.61±0.23	1.15±0.59	1.05±0.53	2.04±0.35	0.46±0.33
1b	4.16±1.07	1.01±0.11	0.89±0.18	1.37±0.24	6.80±0.33	0.15±0.11
2	2.26±0.66	0.58±0.05	0.81±0.12	0.51±0.07	22.07±0.77	0.45±0.08
3	—	0.27±0.07	0.80±0.23	0.44±0.14	16.36±1.18	0.69±0.16
4a	—	—	0.66±0.16	0.47±0.10	7.83±0.40	0.71±0.12
4b	—	—	0.82±0.22	0.57±0.15	22.58±1.29	0.34±0.14
5	—	—	0.91±0.56	—	2.70±0.31	0.34±0.32
6	—	1.42±0.06	0.48±0.08	0.62±0.07	19.92±0.53	1.12±0.06
7a	—	0.48±0.09	0.85±0.23	0.66±0.19	5.37±0.38	0.46±0.15
7b	—	0.27±0.02	0.88±0.11	0.66±0.08	35.97±0.98	0.45±0.06
8	2.21±0.48	0.14±0.02	0.71±0.11	0.66±0.08	28.12±0.70	0.32±0.07
9	—	0.05±0.01	0.77±0.13	0.60±0.09	20.06±0.56	0.11±0.08
10a	—	0.16±0.03	1.07±0.17	0.80±0.13	18.14±0.63	0.46±0.09
10b	—	0.17±0.02	1.01±0.13	0.70±0.08	33.81±0.96	0.64±0.07
11	—	0.47±0.08	1.17±0.27	1.14±0.26	8.42±0.55	0.90±0.14
12	—	—	0.85±0.36	0.79±0.34	4.94±0.62	0.93±0.26
13	—	0.35±0.04	1.04±0.15	0.60±0.09	11.16±0.38	1.23±0.08
14a	—	1.15±0.10	0.91±0.16	0.98±0.16	18.31±0.82	0.72±0.10
14b	3.36±0.76	1.18±0.07	0.79±0.11	0.87±0.10	20.25±0.66	0.70±0.07
15a	—	1.68±0.54	0.65±0.51	—	2.47±0.44	0.21±0.40
15b	6.36±2.07	0.89±0.11	0.66±0.18	0.78±0.20	9.32±0.47	0.07±0.13
16a	2.07±0.92	0.32±0.08	0.73±0.20	0.79±0.20	9.31±0.65	0.66±0.15
16b	2.63±0.61	0.21±0.03	0.73±0.12	0.68±0.09	26.12±0.75	0.56±0.07
17a	—	0.25±0.06	0.92±0.25	0.73±0.20	15.98±1.32	0.38±0.16
17b	—	0.32±0.02	1.22±0.11	0.65±0.05	99.43±1.82	0.62±0.05
18	—	—	0.75±0.47	0.89±0.56	3.63±0.66	1.32±0.38
19	7.54±2.31	0.23±0.07	0.72±0.20	0.82±0.20	13.78±0.88	0.71±0.14
20	—	0.24±0.08	1.11±0.25	0.89±0.21	8.53±0.57	1.06±0.13
21	—	0.30±0.05	1.73±0.31	0.94±0.20	8.93±0.43	0.35±0.12
22	1.78±0.29	0.53±0.02	0.81±0.08	0.60±0.05	22.86±0.44	0.49±0.05
23	1.88±0.25	0.68±0.02	0.85±0.08	0.60±0.04	42.42±0.74	0.09±0.04
24	—	0.76±0.20	1.33±0.52	1.24±0.52	3.62±0.42	0.84±0.25
25	—	0.82±0.16	0.87±0.25	0.71±0.22	5.12±0.41	0.86±0.17
26	—	0.47±0.22	1.34±0.64	1.13±0.55	5.96±0.93	0.92±0.32
27	—	0.72±0.22	1.39±0.56	1.21±0.54	4.56±0.44	0.50±0.25
28	2.37±0.40	0.70±0.03	0.89±0.09	0.69±0.08	38.60±0.81	0.08±0.05
NGC 6217						
1	1.87±0.81	0.25±0.05	0.85±0.16	0.52±0.10	21.24±0.86	0.10±0.10
2	—	—	1.09±0.52	0.89±0.42	7.37±1.14	0.76±0.31

^a *I*(λ)/*I*(H β) ratio. ^b The fluxes are in units of 10⁻¹⁶ erg s⁻¹ cm⁻².

Table 4. Continued

H II region	[O II] ^a 3727+3729	[O III] ^a 5007	[N II] ^a 6584	[S II] ^a 6717+6731	<i>F</i> (H β) ^b 4861	<i>c</i> (H β)
NGC 6217						
3	—	0.98±0.31	1.08±0.43	0.71±0.29	7.70±1.03	0.80±0.25
NGC 7331						
1	—	1.05±0.22	1.20±0.57	0.91±0.44	3.16±0.36	0.09±0.28
2	—	—	2.65±2.33	0.91±0.90	1.13±0.31	1.53±0.68
3	—	0.14±0.06	0.44±0.16	0.26±0.09	9.27±0.79	1.24±0.17
4	2.32±1.15	0.41±0.04	0.99±0.14	0.82±0.10	26.64±0.88	0.50±0.08
NGC 7678						
1	—	1.17±0.58	0.82±0.68	0.88±0.71	3.03±0.81	0.94±0.51
2	—	0.52±0.14	1.01±0.36	0.83±0.29	6.34±0.59	0.32±0.21
3	2.74±0.91	0.30±0.05	0.48±0.13	0.67±0.14	28.74±1.30	0.14±0.10
4	2.00±0.54	0.49±0.05	0.74±0.13	0.60±0.10	29.05±1.10	0.30±0.08
5	4.07±1.78	0.39±0.12	1.47±0.42	0.77±0.27	7.57±0.60	0.06±0.19
6	—	0.31±0.08	1.05±0.24	0.97±0.21	9.54±0.61	0.77±0.14
7	—	0.63±0.03	0.89±0.09	0.85±0.06	61.66±1.21	0.69±0.05
8a	—	0.54±0.02	0.85±0.08	0.69±0.04	196.70±3.16	0.80±0.04
8b	—	0.50±0.02	0.91±0.08	0.62±0.04	101.40±1.63	0.90±0.04
9	—	0.67±0.04	1.04±0.13	0.63±0.08	17.35±0.52	0.79±0.07
10	2.53±0.44	0.44±0.02	0.95±0.10	0.93±0.08	41.05±0.81	0.71±0.05

^a $I(\lambda)/I(\text{H}\beta)$ ratio. ^b The fluxes are in units of 10^{-16} erg s⁻¹ cm⁻².**Figure 3.** Comparison between redding-corrected fluxes $[\text{O III}]\lambda 5007/\text{H}\beta$ obtained in the present paper and data from the literature (Belley & Roy 1992; Rosales-Ortega et al. 2011; van Zee et al. 1998; Bresolin et al. 1999) for common H II regions.

servations in every galaxy: one object in NGC 628 observed by van Zee et al. (1998) and one object in NGC 7331 observed by Bresolin et al. (1999). In Fig. 3 we compared our measurements with results of these two previous spectroscopic observations, with results of the spectrophotometric imaging (Belley & Roy 1992), which are not as accurate as spectroscopic ones for individual

objects, and with results of the Integral Field Spectroscopy for NGC 628 (one object (Rosales-Ortega et al. 2011)) (see Table 3).

Fig. 3 shows a satisfactory agreement between our spectroscopy and previous observations. Note that for the quantitative analysis more statistics is necessary. Previous spectroscopic observations of H II regions in NGC 628 and NGC 7331 will be also compared in Section 3 via radial oxygen and nitrogen abundances distributions in disks of parent galaxies.

3 ABUNDANCES

Here we use the spectral data, presented in Section 2 for the determination of the oxygen and nitrogen abundances (and electron temperatures) in H II regions aiming to establish the radial distributions of these elements across the disks of galaxies.

3.1 Preliminary remarks

Since our measurements of the $[\text{N II}]\lambda 6584$ and $[\text{O III}]\lambda 5007$ lines are more reliable than those of the $[\text{N II}]\lambda 6548$ and $[\text{O III}]\lambda 4959$ lines, we used $[\text{N II}]\lambda 6584$ and $[\text{O III}]\lambda 5007$ lines only. The $[\text{O III}]\lambda 5007$ and $\lambda 4959$ lines originate from transitions from the same energy level, so their fluxes ratio is due only to the transition probability ratio which is 3.013 (Storey & Zeippen 2000). Hence, the value of R_3 can be well approximated by

$$R_3 = 1.33 I_{[\text{O III}]\lambda 5007}/I_{\text{H}\beta}. \quad (5)$$

Similarly, the $[\text{N II}]\lambda 6584$ and $\lambda 6548$ lines also originate from transitions from the same energy level and the transition probability ratio for those lines is 3.071 (Storey & Zeippen 2000). The value of N_2 is therefore well approximated by

$$N_2 = 1.33 I_{[\text{N II}]\lambda 6584}/I_{\text{H}\beta}. \quad (6)$$

We have used Eq.(6) instead of Eq.(2) to obtain the value of N_2 and Eq.(5) instead of Eq.(4) to determine the value of R_3 .

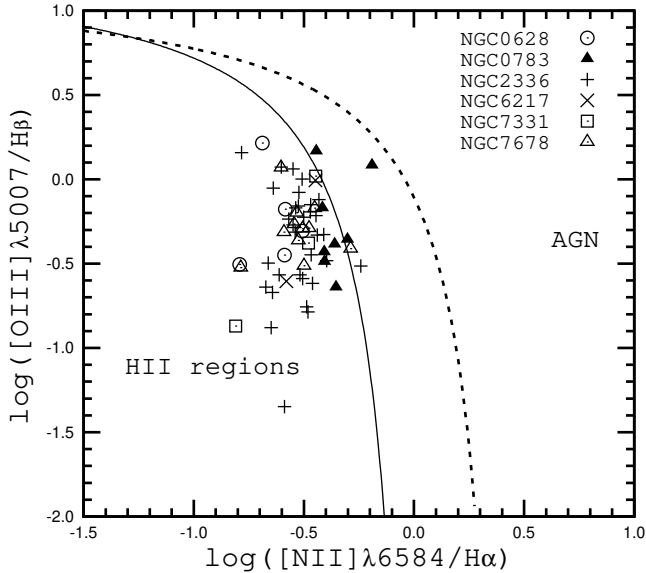


Figure 4. The $[\text{N II}]\lambda 6584/\text{H}\alpha$ versus $[\text{O III}]\lambda 5007/\text{H}\beta$ diagram. The symbols are the H II regions. The solid line separates objects with H II spectra from those containing an AGN according to Kauffmann et al. (2003). The dashed line is the separation line from Kewley et al. (2001).

The intensities of strong, easily measured lines can be used to separate different types of emission-line objects according to their main excitation mechanism. Baldwin, Phillips & Terlevich (1981) proposed a diagram (BPT classification diagram) where the excitation properties of H II regions are studied by plotting the low-excitation $[\text{N II}]\lambda 6584/\text{H}\alpha$ line ratio against the high-excitation $[\text{O III}]\lambda 5007/\text{H}\beta$ line ratio.

The $[\text{N II}]\lambda 6584/\text{H}\alpha$ versus $[\text{O III}]\lambda 5007/\text{H}\beta$ diagram is shown in Fig. 4. The symbols are H II regions. The solid line represents the relation

$$\log([\text{O III}]\lambda 5007/\text{H}\beta) = \frac{0.61}{\log([\text{N II}]\lambda 6584/\text{H}\alpha) - 0.05} + 1.3, \quad (7)$$

which separates objects with H II spectra from those containing an AGN (Kauffmann et al. 2003). The dashed separation line is the relation

$$\log([\text{O III}]\lambda 5007/\text{H}\beta) = \frac{0.61}{\log([\text{N II}]\lambda 6584/\text{H}\alpha) - 0.47} + 1.19 \quad (8)$$

from Kewley et al. (2001). Fig. 4 shows that all H II regions from our sample are thermally photoionised objects if the separation line from Kewley et al. (2001) is used. When the separation line from Kauffmann et al. (2003) is used then one object (No. 7 in NGC 783) has an appreciable shift from the separation line towards the AGNs. However the uncertainty in the measurement of the intensity of the $[\text{N II}]\lambda 6584$ line is large for this object (see Table 4). Therefore all H II regions are included in further consideration. The abundances determined for object No. 7 from NGC 783 are not considered in question.

3.2 Abundances and temperatures

Accurate oxygen and nitrogen abundances in H II regions can be derived via the classic T_e method, often referred to as the direct method. This method is based on the measurement of the electron temperature t_3 within the $[\text{O III}]$ zone and/or the electron temperature t_2 within the $[\text{N II}]$ zone. The ratio of the nebular to auroral

oxygen line intensities $[\text{O III}](\lambda 4959 + \lambda 5007)/[\text{O III}]\lambda 4363$ is usually used for the t_3 determination, while the ratios of the nebular to auroral nitrogen line intensities $[\text{N II}](\lambda 6548 + \lambda 6584)/[\text{N II}]\lambda 5755$ or $[\text{O II}](\lambda 3727 + \lambda 3729)/[\text{O II}](\lambda 7320 + \lambda 7330)$ are used for the t_2 determination. The auroral lines in spectra of H II regions from our sample are too faint to be detected. In this case, it is still possible to obtain the estimates of the nebular abundances, using intensity ratios of the brightest ionic emission lines.

Pagel et al. (1979) and Alloin et al. (1979) have suggested that the locations of H II regions in some emission-line diagrams can be calibrated in terms of their oxygen abundances. This approach to abundance determination in H II regions, usually referred to as the "strong line method" has been widely adopted, especially in the cases where the temperature-sensitive auroral lines are not detected. Numerous relations have been proposed to convert metallicity-sensitive emission-line ratios into metallicity or temperature estimates (e.g. Dopita & Evans 1986; Zaritsky et al. 1994; Vilchez & Esteban 1996; Pilyugin 2000, 2001; Pettini & Pagel 2004; Tremonti et al. 2004; Pilyugin & Thuan 2005; Liang et al. 2006; Stasińska 2006; Thuan et al. 2010). (See the review in Ellison et al. (2008); López-Sánchez & Esteban (2010) for more details).

Two calibration relations for estimation of the oxygen and nitrogen abundances in H II regions have been recently suggested. The ON-calibration relations give the oxygen and nitrogen abundances and electron temperature in terms of the fluxes of the strong emission lines O^{++} , O^+ , and N^+ (Pilyugin et al. 2010). The NS-calibration relations give abundances and electron temperatures in terms of the fluxes in the strong emission lines of O^{++} , N^+ , and S^+ (Pilyugin & Mattsson 2011). The ON and NS calibrations provide reliable oxygen and nitrogen abundances for H II regions of all metallicities. The oxygen R_2 line is measured in presented spectra with a large uncertainty (or even not available). Therefore we use the NS calibration method to estimate the abundances and electron temperatures in our sample of H II regions.

Both individual H II regions, excited by a single source (single star or star cluster), and giant H II regions can be observed in nearby galaxies. Giant H II regions can be composite nebulae which contain a number of H II regions with different physical properties, all contributing to the global spectrum (Kennicutt 1984). The ON and NS calibrations give oxygen and nitrogen abundances in composite nebulae which agree with the mean luminosity-weighted abundances of their components to within ~ 0.2 dex (Pilyugin et al. 2012).

The calibrations are constructed under the assumption that the H II regions are in the low-density regime. Since the sulphur lines $[\text{S II}]\lambda 6717$ and $[\text{S II}]\lambda 6731$ in most of our spectra are blended (the $[\text{S II}]\lambda 6717$ and $[\text{S II}]\lambda 6731$ were deblended in a several cases only and with a low accuracy), we cannot estimate the density sensitive ratio $[\text{S II}]\lambda 6717/[\text{S II}]\lambda 6731$ and verify the low-density regime in our objects. Therefore we assume that the H II regions of our sample are all in the low-density regime, which is typical for the majority of extragalactic H II regions (Zaritsky et al. 1994; Bresolin et al. 2005; Gutiérrez & Beckman 2010).

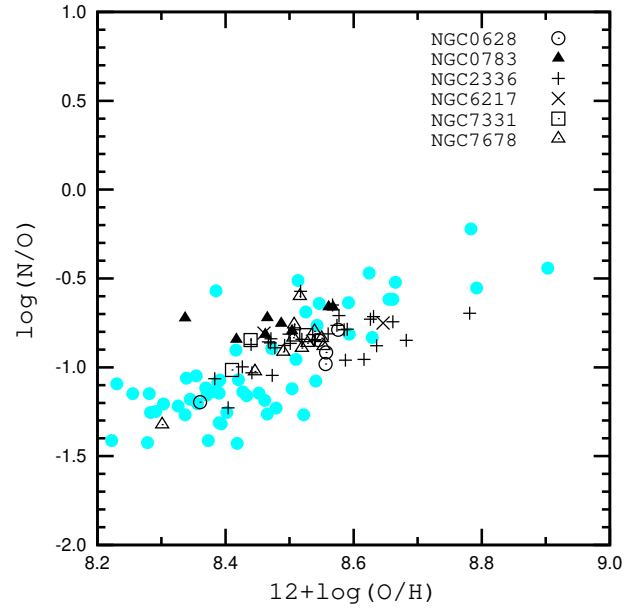
In previous works, a little attention was paid to the radial distribution of nitrogen abundances in the disks of spiral galaxies, despite the fact that such studies would have several advantages (Thuan et al. 2010). First, since at $12 + \log(\text{O}/\text{H}) \gtrsim 8.3$, secondary nitrogen becomes dominant and the nitrogen abundance increases at a faster rate than the oxygen abundance (Henry et al. 2000), the change in nitrogen abundances with galactocentric distance should show a larger amplitude in comparison to oxygen abundances and,

Table 5. Oxygen and nitrogen abundances and electron temperatures t_2 in H II regions derived using the NS calibrations.

H II region	R_G^a	$12+\log(\text{O}/\text{H})_{\text{NS}}$	$12+\log(\text{N}/\text{H})_{\text{NS}}$	t_{NS}^b
NGC 628				
4	0.25	8.36	7.16	0.77
7	0.37	8.58	7.79	0.74
8	0.48	8.55	7.70	0.77
9	0.49	8.56	7.57	0.82
10	0.57	8.56	7.64	0.75
NGC 783				
1	0.73	8.42	7.57	0.88
3	0.57	8.56	7.90	0.71
4	0.82	8.46	7.65	0.81
6	0.77	8.46	7.74	0.79
7	0.84	8.34	7.61	0.91
8	0.58	8.57	7.91	0.72
NGC 2336				
1a	0.88	8.47	7.61	0.81
1b	0.88	8.38	7.32	0.91
2	0.72	8.56	7.75	0.75
3	0.48	8.66	7.92	0.68
6	0.98	8.40	7.18	0.88
7a	0.65	8.54	7.69	0.76
7b	0.65	8.59	7.80	0.71
8	0.55	8.68	7.83	0.66
9	0.44	8.78	8.09	0.59
10a	0.50	8.63	7.90	0.68
10b	0.50	8.63	7.92	0.68
11	0.45	8.47	7.63	0.80
13	0.63	8.58	7.87	0.72
14a	0.97	8.43	7.43	0.88
14b	0.97	8.44	7.41	0.87
15b	0.79	8.47	7.43	0.84
16a	0.52	8.59	7.63	0.73
16b	0.52	8.64	7.76	0.69
17a	0.60	8.59	7.80	0.71
17b	0.60	8.57	7.92	0.72
19	0.56	8.62	7.66	0.71
20	0.62	8.57	7.81	0.72
21	0.57	8.52	7.94	0.74
22	0.76	8.54	7.69	0.76
23	0.74	8.52	7.68	0.78
24	0.66	8.44	7.57	0.84
25	0.65	8.48	7.59	0.82
26	0.53	8.50	7.69	0.78
27	0.55	8.47	7.61	0.81
28	0.86	8.50	7.64	0.79
NGC 6217				
1	0.48	8.65	7.89	0.68
3	0.47	8.46	7.65	0.83
NGC 7331				
1	0.49	8.44	7.59	0.85
3	0.17	8.41	7.39	0.69
4	0.45	8.53	7.71	0.76
NGC 7678				
1	0.90	8.45	7.42	0.87
2	0.59	8.51	7.67	0.78
3	0.56	8.30	6.98	0.80
4	0.56	8.55	7.67	0.76
5	0.56	8.52	7.92	0.75
6	0.49	8.55	7.71	0.74
7	0.67	8.49	7.58	0.80
8a	0.59	8.53	7.66	0.77
8b	0.59	8.54	7.74	0.76

Table 5. Continued

H II region	R_G^a	$12+\log(\text{O}/\text{H})_{\text{NS}}$	$12+\log(\text{N}/\text{H})_{\text{NS}}$	t_{NS}^b
9	0.82	8.51	7.75	0.78
10	0.38	8.52	7.63	0.77

^a in unit of isophotal radius R_{25} .^b t_2 in unit of 10^4 K.**Figure 5.** The O/H–N/O diagram. The different symbols marked in the legend show abundances derived using the NS-calibration for our sample of H II regions. The filled circles show T_e -based abundances in the sample of best-studied H II regions in nearby galaxies (the compilation of data from Pilyugin et al. (2010)).

as a consequence, the gradient (and differences in gradients among galaxies) should be easier to detect. Furthermore, there is a time delay in the nitrogen production as compared to oxygen production (Maeder 1992; van den Hoek & Groenewegen 1997; Pagel 1997; Pilyugin & Thuan 2011). This provides an additional constraint on the chemical evolution of galaxies. For these reasons, not only the radial distribution of oxygen abundances but also that of nitrogen abundances are estimated here.

The resultant NS calibration abundances and electron temperatures are given in Table 5. The oxygen and nitrogen abundances and electron temperature were derived for H II regions where R_3 , N_2 , and S_2 lines are available. It should be noted that the NS-calibration relations have been derived using spectra of H II regions with well-measured electron temperatures as calibration datapoints. Therefore, the NS-calibration relations produce the abundances which are in agreement with the abundance scale defined by the classic T_e method.

The O/H–N/O diagram gives a possibility to test the validity of the determined abundances. On the O/H–N/O diagram (Fig. 5) we compare abundances of 50 H II regions in six studied galaxies (see legend) with T_e -based abundances of the best studied H II regions (open circles) in nearby galaxies (data compiled from Pilyugin et al. (2010)). One can see from Fig. 5, that all points lie within the spread of Pilyugin et al. (2010), i.e. the abundances in

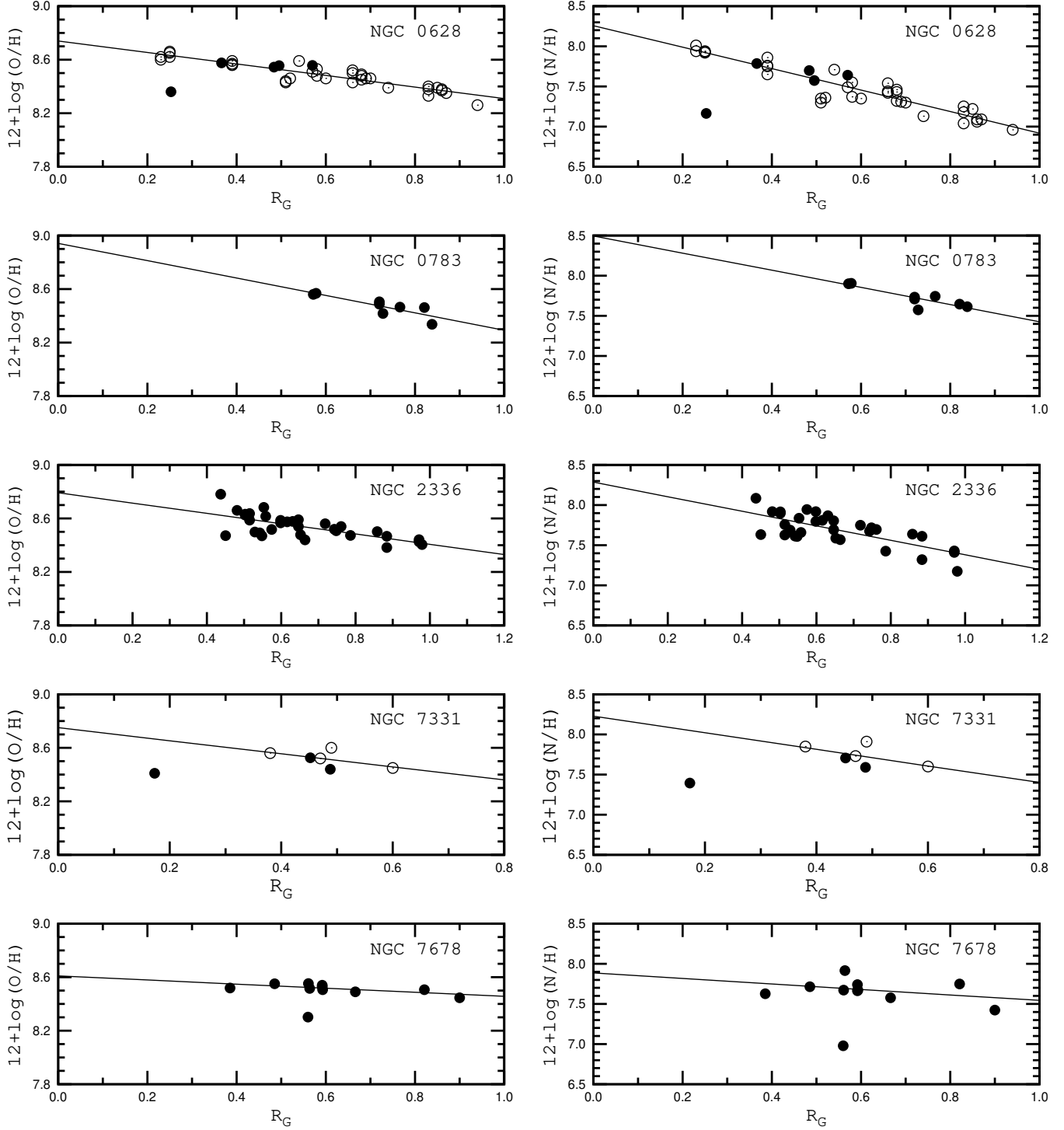


Figure 6. Radial distributions of oxygen abundances (left column panels) and nitrogen abundances (right column panels) in the disks of galaxies. Filled circles are abundances estimated from our observational data, open circles are abundances based on the line measurements from the literature. The solid lines are best fits to these datapoints.

our sample of H II regions derived using the NS-calibration occupy the same band in the O/H - N/O diagram as the T_e -based abundances in the sample of best-studied H II regions in nearby galaxies. This shows that our abundance estimations based on the NS-calibration method are realistic.

3.3 Radial abundance gradients

It is common practice (e.g. Zaritsky et al. 1994; van Zee et al. 1998; Pilyugin et al. 2004) that the radial oxygen abundance distribution in the disk of spiral galaxy is fitted by the expression of the type:

$$12 + \log(\text{O}/\text{H}) = 12 + \log(\text{O}/\text{H})_0 + C_{\text{O}/\text{H}} \times (R/R_{25}), \quad (9)$$

Table 6. Parameters of radial distributions of oxygen and nitrogen abundances in the disks of galaxies.

galaxy	O/H center ^a	O/H gradient ^b	N/H center ^a	N/H gradient ^b
NGC 628	8.74 ± 0.02	-0.43 ± 0.03	8.26 ± 0.05	-1.34 ± 0.08
NGC 783	8.94 ± 0.12	-0.65 ± 0.16	8.49 ± 0.19	-1.07 ± 0.26
NGC 2336	8.79 ± 0.05	-0.38 ± 0.07	8.25 ± 0.10	-0.90 ± 0.15
NGC 7331	8.75 ± 0.18	-0.49 ± 0.36	8.23 ± 0.36	-1.03 ± 0.74
NGC 7678	8.61 ± 0.03	-0.15 ± 0.05	7.89 ± 0.17	-0.34 ± 0.27

^a in unit of $12 + \log(X/H)$.^b in unit of dex/ R_{25} .

where $12 + \log(O/H)_0$ is the extrapolated central oxygen abundance, $C_{O/H}$ is the slope of the oxygen abundance gradient expressed in terms of dex/ R_{25} , and R/R_{25} is the fractional radius (the galactocentric distance normalized to the disk isophotal radius). Analogously to the case of the oxygen abundance, the radial nitrogen abundance distribution in the disk of spiral galaxy is fitted by the equation of the type:

$$12 + \log(N/H) = 12 + \log(N/H)_0 + C_{N/H} \times (R/R_{25}). \quad (10)$$

Fig. 6 shows the radial oxygen (left column of panels) and nitrogen (right column of panels) abundances distributions in the disk of spiral galaxies NGC 628, NGC 783, NGC 2336, NGC 7331, and NGC 7678. The abundances derived from our spectral data are shown by the filled circles.

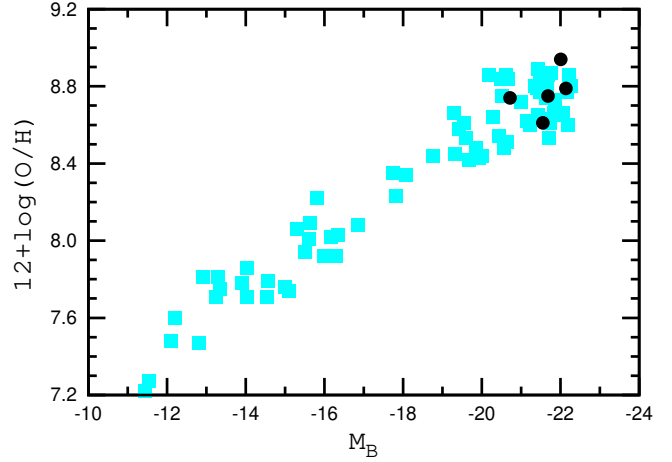
The emission line measurements in the spectra of H II regions in the disk of the galaxy NGC 628 previously were reported by McCall et al. (1985); Ferguson et al. (1998); van Zee et al. (1998); Bresolin et al. (1999) and in the disk of the galaxy NGC 7331 were given by McCall et al. (1985); Ferguson et al. (1998).

As noted in Section 2.3, there are only two objects in NGC 628 and NGC 7331 in common with previous spectroscopic observations. Nevertheless the abundances estimations in NGC 628 and NGC 7331 can be directly compared with previously published ones. First we estimated the oxygen and nitrogen abundances through the NS calibration, using previously published line measurements. Further, we plotted these estimations on the diagram of the radial distributions of oxygen and nitrogen abundances in the disks of NGC 628 and NGC 7331 together with our abundances estimations.

The galactocentric distances were recomputed with the inclinations and position angles adopted here (Table 1).

Fig. 6 shows a good agreement in the radial abundances distribution in NGC 628 and NGC 7331 between H II regions observed in present paper (filled circles) and H II regions observed previously (open circles) in these galaxies.

The numerical values of the coefficients in Eq.(9) ($C_{O/H}$ and $12 + \log(O/H)_0$) and in Eq.(10) ($C_{N/H}$ and $12 + \log(N/H)_0$) have been derived through the least squares method. Both our data and data from the literature are used. If there are datapoints which deviate significantly (more than 3σ) from the general trend, then these points were excluded in the derivation of the final relations. The obtained relations are presented on the Fig. 6 by the solid lines. Computed parameters of radial distributions of oxygen and nitrogen abundances (the numerical values of the coefficients in Eq.(9) and

**Figure 7.** The luminosity – central metallicity diagram. The dark (black) circles denote the central abundances in the disks of spiral galaxies from the present sample. The grey (blue) squares show the central abundances in the disks of spiral galaxies and abundances in irregular galaxies from Pilyugin et al. (2007). (A colour version of this figure is available in the online version.)

Eq.(10)) in the disks of galaxies NGC 628, NGC 783, NGC 2336, NGC 7331, and NGC 7678 are listed in Table 6.

3.4 Discussion

Examination of Fig. 6 shows that the radial distributions of the oxygen and nitrogen abundances in the disks of considered galaxies are fitted well by the single linear expression within the optical isophotal radius. The variation of nitrogen abundances with galactocentric distance shows a larger amplitude in comparison to oxygen abundances and the differences in nitrogen abundance gradients among galaxies are larger than that in oxygen abundance gradients.

The luminosity – central metallicity diagram for spiral and irregular galaxies have been constructed in Pilyugin et al. (2007). The abundances of H II regions in that paper and here have been estimated through the methods producing the abundances which are in agreement with the abundance scale defined by the classic T_e method. Therefore the abundances obtained in these studies can be compared. Fig. 7 shows the luminosity – central metallicity diagram. The grey (blue) squares show the central abundances in the disks of spiral galaxies and abundances in irregular galaxies from Pilyugin et al. (2007). The dark (black) circles denote the central abundances in the disks of spiral galaxies from the present sample. The absolute blue magnitudes M_B are taken from the LEDA data base. Inspection of Fig. 7 shows that our sample of galaxies follows well the general trend in the luminosity – central metallicity diagram for spiral and irregular galaxies.

4 CONCLUSIONS

The spectroscopic observations of H II regions in six spiral galaxies (NGC 628, NGC 783, NGC 2336, NGC 6217, NGC 7331, and NGC 7678) obtained with the 6-meter telescope of Special Astrophysical Observatory (SAO) of the Russian Academy of Sciences were carried out.

The oxygen and nitrogen abundances as well the electron temperatures in 50 H II regions are estimated using the recent version of

the strong line method (the NS-calibration). The parameters of the radial distributions (the extrapolated central intercept value and the gradient) of the oxygen and nitrogen abundances in the disks of the NGC 628, NGC 783, NGC 2336 and NGC 7678 are obtained. The oxygen and nitrogen abundances and their gradients in the disks of spiral galaxies NGC 783, NGC 2336, and NGC 7678 are estimated for the first time. The abundances for the NGC 6217 are also found for the first time.

Galaxies from our sample follow well the general trend in the luminosity – central metallicity diagram for spiral and irregular galaxies.

ACKNOWLEDGMENTS

We are grateful to the referee for his/her constructive comments. L.S.P. acknowledges support from the Cosmomicrophysics project of the National Academy of Sciences of Ukraine. A.S.G. is grateful to A.Y. Kniazev (South African Astronomical Observatory), to L.V. Afanasiev and A.V. Moiseev (Special Astrophysical Observatory) for help and support during the observations in SAO and for fruitful discussion, to A.V. Zasov and B.P. Artamonov (Sternberg Astronomical Institute) for useful discussions. The authors acknowledge the usage of the HyperLeda data base (<http://leda.univ-lyon1.fr>). This study was supported in part by the Russian Foundation for Basic Research (project nos. 08–02–01323, 10–02–91338, and 12–02–00827). Results based on observations collected with the 6-m telescope of the Special Astrophysical Observatory (SAO) of the Russian Academy of Sciences (RAS), operated under the financial support of the Science Department of Russia (registration number 01–43).

REFERENCES

- Afanasiev L.V., Moiseev A.V. 2005, *Astron. Lett.*, 31, 193
 Alloin D., Collin-Souffrin S., Joly M., Vigroux L. 1979, *A&A*, 78, 200
 Artamonov B.P., Badan Yu.Yu., Bruyevich V.V., Gusev A.S. 1999, *Astron. Rep.*, 43, 377
 Artamonov B.P., Bruyevich V.V., Gusev A.S. 1997, *Astron. Rep.*, 41, 577
 Baldwin J.A., Phillips M.M., Terlevich R. 1981, *PASP*, 93, 5
 Belley J., Roy J.-R. 1992, *ApJS*, 78, 61
 Bresolin F., Kennicutt R.C., Garnett D.R. 1999, *ApJ*, 510, 104
 Bresolin F., Schaerer D., Conzález Delgado R.M., Stasińska G. 2005, *A&A*, 441, 981
 Bresolin F., Gieren W., Kudritzki R.-P., Pietrzyński G., Urbaneja M.A., Carraro G. 2009, *ApJ*, 700, 309
 Bruyevich V.V., Gusev A.S., Ezhkova O.V., Sakhibov F.Kh., Smirnov M.A. 2007, *Astron. Rep.*, 51, 222
 Chiappini V., Romano D., Matteucci F. 2003, *MNRAS*, 339, 63
 Dinerstein H.L. 1990, in "The Interstellar Medium in Galaxies" eds. H.A. Thronson (Jr.) and J.M. Shull (Dordrecht: Kluwer), 257
 Dopita M.A., Evans I.N. 1986, *ApJ*, 307, 431
 Dutil D.R., Roy J.-R. 1999, *ApJ*, 516, 62
 Ellison S.L., Patton D.R., Simard L., McConnachie A.W. 2008, *AJ*, 135, 1877
 Ferguson A.M.N., Gallagher J.S., Wyse R.F.G. 1998, *AJ*, 116, 673
 Garnett D.R., Shields G.A. 1987, *ApJ*, 317, 82
 Garnett D.R. 2002, *ApJ*, 581, 1019
 Gusev A.S. 2006a, *Astron. Rep.*, 50, 167
 Gusev A.S. 2006b, *Astron. Rep.*, 50, 182
 Gusev A.S., Park M.-G. 2003, *A&A*, 410, 117
 Gutiérrez L., Beckman J.E. 2010, *ApJ*, 710, L44
 Henry R.B.C., Edmunds M.G., Kóppen J. 2000, *ApJ*, 541, 660
 Izotov Y.I., Thuan T.X., Lipovetsky V.A. 1994, *ApJ*, 435, 647
 Izotov Y.I., Stasińska G., Guseva N.G., Thuan T.X. 2004, *A&A*, 415, 87
 Kartasheva T.A., Chunakova N.M. 1978, *Izv. SAO*, 10, 44
 Kauffmann G., Heckman T.M., Tremonti C., et al. 2003, *MNRAS*, 346, 1055
 Kennicutt R.C. 1984, *ApJ*, 287, 116
 Kennicutt R.C., Bresolin F., Garnett D.R. 2003, *ApJ*, 591, 801
 Kewley L.J., Dopita M.A., Sutherland R.S., Heisler C.A., Trevena J. 2001 *ApJ*, 556, 121
 Liang Y.C., Yin S.Y., Hammer F., Deng L.C., Flores H., Zhang B. 2006, *ApJ*, 652, 257
 López-Sánchez Á.R., Esteban C. 2010, *A&A*, 517, A85
 Maeder A. 1992, *A&A*, 264, 105
 Marcon-Uchida M.M., Matteucci F., Costa, R.D.D. 2010, *A&A*, 520, A35
 McCall, M. L., Rybski, P. M., Shields, G. A. 1985, *ApJS*, 57, 1
 Moustakas J., Kennicutt R.C. (Jr), Tremonti C.A., Dale D.A., Smith J.-D.T., Calzetti D. 2010, *ApJS*, 190, 233
 Oke J.B. 1990, *AJ*, 99, 1621
 Osterbrock D.E. 1989, *Astrophysics of gaseous nebulae and active galactic nuclei* (Mill Valley, CA: University Science Books), 422 p.
 Pagel B. E. J., Edmunds M. G., Blackwell D. E., Chun M. S., Smith G. 1979, *MNRAS*, 189, 95
 Pagel B.E.J. 1991, *Nuclei in the Cosmos*, ed. H. Oberhummer (Berlin: Springer), 89
 Pagel B.E.J., 1997, *Nucleosynthesis and Chemical Evolution of Galaxies* (Cambridge: Cambridge Univ. Press), 392 p.
 Paturel G., Petit C., Prugniel Ph., Theureau G., Rousseau J., Brouty M., Dubois P., Cambresy L. 2003, *A&A*, 412, 45
 Pettini, M., Pagel, B.E.J. 2004, *MNRAS*, 348, 59L
 Pilyugin L.S. 2000, *A&A*, 362, 325
 Pilyugin L.S. 2001, *A&A*, 369, 594
 Pilyugin L.S., Vílchez J.M., Contini T. 2004, *A&A*, 425, 849
 Pilyugin L.S., Thuan T.X. 2005, *ApJ*, 631, 231
 Pilyugin L.S., Thuan T.X., Vílchez J.M. 2007, *MNRAS*, 376, 353
 Pilyugin L.S., Vílchez J.M., Thuan T.X. 2010, *ApJ*, 720, 1738
 Pilyugin L.S., Thuan T.X. 2011, *ApJ*, 726, L23
 Pilyugin L.S., Mattsson L. 2011, *MNRAS*, 412, 1145
 Pilyugin L.S., Vílchez J.M., Mattsson L., Thuan T.X. 2012, *MNRAS*, 421, 1624
 Rosales-Ortega F.F., Diaz A.I., Kennicutt R.C., Sanchez S.F. 2011, *MNRAS*, 415, 2439
 Roy J.-R., Belley J., Dutil Y., Martin P. 1996, *ApJ*, 460, 294
 Searle L. 1971, *ApJ*, 168, 327
 Stasińska G. 2006, *A&A*, 454, L127
 Storey P.J., Zeippen C.J. 2000, *MNRAS*, 312, 813
 Thuan T.X., Pilyugin L.S., Zinchenko I.A. 2010, *ApJ*, 712, 1029
 Tremonti C.A., Heckman T.M., Kauffmann G., et al. 2004, *ApJ*, 613, 898
 van den Hoek L.B., Groenewegen M.A.T. 1997, *A&AS*, 123, 305
 van Zee L., Salzer J.J., Haynes M.P., O'Donoghue A.A., Balonek T.J. 1998, *AJ*, 116, 2805
 Vila-Costas M.B., Edmunds M.G. 1992, *MNRAS*, 259, 121
 Vílchez J.M., Esteban C. 1996, *MNRAS*, 280, 720
 Zaritsky D., Kennicutt R.C., Huchra J.P. 1994, *ApJ*, 420, 87